

# D-shaped fiber grating refractive index sensor induced by an ultrashort pulse laser

CHANGRUI LIAO,<sup>1,†</sup> QIAO WANG,<sup>1,†</sup> LEI XU,<sup>2</sup> SHEN LIU,<sup>1</sup> JUN HE,<sup>1</sup> JING ZHAO,<sup>1</sup>  
ZHENGYONG LI,<sup>1</sup> AND YIPING WANG<sup>1,\*</sup>

<sup>1</sup>Key Laboratory of Optoelectronic Devices and Systems of Ministry of Education and Guangdong Province, College of Optoelectronic Engineering, Shenzhen University, Shenzhen 518060, China

<sup>2</sup>School of Electronic and Communication Engineering, Shenzhen Polytechnic, Shenzhen 518055, China

\*Corresponding author: ypwang@szu.edu.cn

Received 30 November 2015; revised 26 January 2016; accepted 27 January 2016; posted 28 January 2016 (Doc. ID 254771); published 23 February 2016

The fabrication of fiber Bragg gratings was here demonstrated using ultrashort pulse laser point-by-point inscription. This is a very convenient means of creating fiber Bragg gratings with different grating periods and works by changing the translation speed of the fiber. The laser energy was first optimized in order to improve the spectral properties of the fiber gratings. Then, fiber Bragg gratings were formed into D-shaped fibers for use as refractive index sensors. A nonlinear relationship was observed between the Bragg wavelength and liquid refractive index, and a sensitivity of  $\sim 30$  nm/RIU was observed at 1.450. This shows that D-shaped fiber Bragg gratings might be used to develop promising biochemical sensors. © 2016 Optical Society of America

**OCIS codes:** (060.3735) Fiber Bragg gratings; (060.2370) Fiber optics sensors; (140.7090) Ultrafast lasers.

<http://dx.doi.org/10.1364/AO.55.001525>

## 1. INTRODUCTION

Fiber Bragg gratings (FBGs), which have been studied for more than 30 years, have become ubiquitous in optical telecommunications and optical fiber sensors [1]. Point-by-point (PBP) FBG inscription was first demonstrated in 1993 using an excimer laser [2], but this drew little interest from researchers until the advent of ultrashort pulse laser micromachining. Recently, the use of ultrashort pulse laser for FBG fabrication has gained more and more interest because of the increasing availability of commercial turn-key ultrashort pulse laser systems, and the requirement that FBGs be included in special fibers. Unlike the frequently used phase-mask method, PBP inscription has a few advantages, specifically good fabrication flexibility, high machining efficiency, and low cost because it does not require an expensive phase mask [3–5]. Recently, PBP inscription of FBGs using ultrashort pulse lasers has been successfully realized in single-mode fibers (SMFs) [4–8], rare-earth doped fibers [9], and microstructured fibers [10].

D-shaped fiber supports a very important platform for the development of novel fiber sensors. The large evanescent field makes the modal propagation constant of the fiber become sensitive to the surrounding refractive index. Recently, various of D-shaped FBG sensors have been reported, i.e., surface-relief D-shaped FBG for 1100°C high temperature sensing [11], polydimethylsiloxane layer covered D-shaped FBG for volatile

organic compound sensing [12], graphene-based D-shaped FBG for erythrocyte detection [13].

In this paper, first FBGs were PBP-inscribed into SMFs using different laser pulse energies, and the morphology and spectral properties of these FBGs were studied to identify the best fabrication parameters, i.e., laser energy and laser focusing conditions. Then, an attempt was made to fabricate FBGs in D-shaped fibers for use as a refractive index sensor. There is a nonlinear relationship between the Bragg wavelength and liquid refractive index (RI), and a sensitivity of  $\sim 30$  nm/RIU was achieved at 1.450. Many “in-fiber” configurations have been presented for RI measurement, i.e., long period fiber gratings (LPFGs) [14], in-fiber surface plasmon resonance (SPR) [15], fiber in-line interferometers [16]. Different from the above methods, the D-shaped FBG can work at “single-end” detection mode, which is more convenient especially for microliter or sub-microliter dose detection. Therefore, this D-shaped FBG might be useful in the development of biochemical sensors.

## 2. DEVICE FABRICATION

Figure 1 shows a schematic diagram of the PBP FBG inscription system. An ultrashort pulsed laser (spectra-physics, solstice) producing 100 fs pulses at 800 nm and a repetition rate of 1 kHz was focused into the fiber core by an oil-immersion microscope objective (MO) with an NA value of 1.25. The

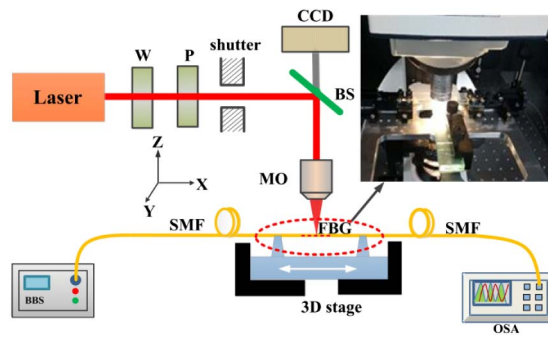


**Fig. 1.** Schematic diagram of ultrashort pulse laser PBP inscription system.

machined fiber is mounted on a high precision 3D translation stage (Newport, XMS50/XMS50/GTS30V) to facilitate control of the translation speed during inscription along the X axis (fiber axis) and correcting displacement along the Y axis, and the height of the fiber is changed along the Z axis. Laser energy is attenuated by rotating a half-wave plate (W) followed by a polarizer (P). A high-speed shutter is used to precisely control laser irradiation time. A broadband light source (BBS) and an optical spectrum analyzer (OSA) are connected to the machined fiber to measure the transmission spectrum in real time. A CCD mounted top is used to monitor fabrication morphology. During inscription, the fiber is moved at a designated speed along the X axis, and each laser pulse produces one grating segment in the core. Because of the multiphoton absorption of the ultrashort pulse laser interaction with silica, fiber photosensitization is not required prior to grating inscription. To avoid the cylindrical lens effect from the surface curvature of fiber, the RI value of the oil used for MO is close to that of silica [17].

Laser energy is the most important parameter in fiber grating inscription. Low laser energy can induce small changes in RI and small modulation area so that the grating length must be increased to achieve satisfactory reflectivity. Conversely, excessively high laser energy can damage large areas of material, and the adjacent grating segment might overlap this damaged area to decrease mode coupling efficiency [18]. Moreover, the laser induced damage will introduce a harmful insertion loss for the sensing system. Experiments were made to find out the optimized laser energy for grating inscription. The fiber was moving at a speed of 2 mm/s to create the grating period of 2  $\mu\text{m}$ , and the laser energy was tested from 0 to 300 nJ. Figure 2 shows the grating morphology from the top view (along the laser beam) and side view where the laser energy is set to be 150, 180, 240, and 300 nJ. It is seen from this figure that the laser induced area is a tiny point at 150 nJ and when the laser energy is increased up to 240 nJ, it turns into a line perpendicular to the fiber axis due to the focusing length of the laser beam. If the laser energy is further increased up to 300 nJ, more than one group of grating is inscribed simultaneously, and they are parallel to each other and the same grating period. This morphology can be explained by the self-focusing effect, where the laser intensity of self-focusing regions keep increasing as the laser beam travels through the fiber until the defocusing effects and material damage interrupt this process

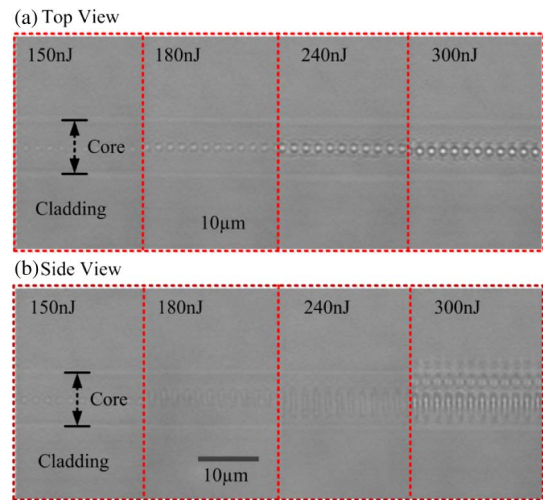


**Fig. 2.** (a) Top-view; (b) side-view optical microscope images of the PBP gratings in SMFs with laser energy 150, 180, 240, and 300 nJ.

[19,20]. In following FBG fabrication, moderate laser energy of  $\sim 240$  nJ is employed to avoid self-focusing effect.

### 3. EXPERIMENT RESULTS AND DISCUSSION

The Bragg wavelength of FBG ( $\lambda_B$ ) can be determined using Eq. (1), where  $m$  is the resonance order;  $n_{\text{eff}}$  is the effective RI of the core mode;  $\nu$  is the translation speed of the fiber; and  $f$  is the repetition rate of the laser.

$$\lambda_B = \frac{2n_{\text{eff}}\nu}{mf}. \quad (1)$$

It is hard to determine the first-order FBGs in the C-band using an 800 nm ultrashort pulse laser because there is a large area of overlap between the adjacent grating segments. Here, the second-order FBG with a grating period of 1.071  $\mu\text{m}$  has been successfully achieved at a speed of 1.071 mm/s with the repetition rate of the ultrashort pulse laser being 1 kHz. The grating length is  $\sim 5$  mm, and the fabrication time is only  $\sim 5$  s, whereas this is usually in the range of min for other FBG fabrication techniques. Figure 3 shows the transmission spectrum of the fabricated FBG, where the Bragg wavelength is  $\sim 1548$  nm; the strength of Bragg resonance is  $\sim 8.1$  dB; the FWHM is  $\sim 0.55$  nm; and the insertion loss is  $\sim 1.96$  dB. Unlike FBGs fabricated using conventional techniques, the cladding mode is very pronounced, which is similar to the spectrum of tilted FBGs. Each resonant peak is produced by the coupling of the core mode to one definite cladding mode characterized by the radial and azimuthal mode numbers. Two sets of resonances with distinct well-defined envelopes, which are denoted by blue and red points, are shown in Fig. 3, and they correspond to two groups of cladding modes [21].

To render the core mode sensitive to surrounding RI change, FBGs were PBP inscribed in D-shaped fibers [11,12], which were side polished from SMF. Figure 4 illustrates a schematic diagram of the wheel polishing system (WanRun, China) [22]. First, a standard SMF with a core/cladding diameter of 8.2/125  $\mu\text{m}$  was fixed by a pair of fiber holders. A 20 g weight was hung to keep constant tension on the polished fiber. The

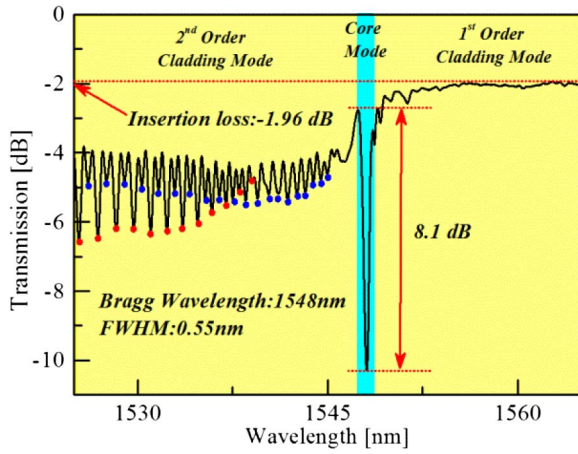


**Fig. 3.** Transmission spectrum of a PBP FBG operating in 2nd order at 1548 nm with strong cladding mode resonance.

polymer coating was stripped in advance over a section of polished length and then cleaned with alcohol. Next, the wheel, wound with abrasive paper, was driven down along the Z direction. Here, the rolling speed of the wheel and moving distance along the Y direction were preset using a personal computer (PC). Then, the unjacketed fiber was gradually polished by back-and-forth movement of the rolling wheel along the Y direction. During the polishing process, the side view of the D-shaped fiber was monitored along the X direction with a microscope. Abrasive paper (12000-mesh, Warriors 991A, STABCKE, Germany) was chosen, and the grit size of this abrasive paper is  $\sim 1 \mu\text{m}$ .

The cross section of D-shaped fiber is shown in Fig. 5(a), where the remaining fiber thickness is  $\sim 66.9 \mu\text{m}$ . The length of the flat region and tapered transition region are  $\sim 8$  and  $\sim 2$  mm, respectively. The polished surface was gently cleaned by ultrasound equipment to wipe off the residual silica dust. Figure 5(b) shows the SEM image of polished surface after ultrasound cleaning, and the surface roughness is  $\sim 1 \mu\text{m}$ . Using the above-mentioned method, PBP FBG with a period of  $1.086 \mu\text{m}$  was then inscribed in the core of the D-shaped fiber with the laser irradiation from the flat surface. Laser energy of 240 nJ was used. The side and front views of the grating are shown in Figs. 5(c) and 5(d), respectively. Because the core is located close to the flat surface of the fiber, it is easy to incorrectly focus on the surface, not in the core, leading to surface damage rather than modifying the core during the inscription. Therefore, the focusing process should be carefully done.

The transmission spectrum of the D-shaped FBG is illustrated in Fig. 6, where the Bragg wavelength is located at

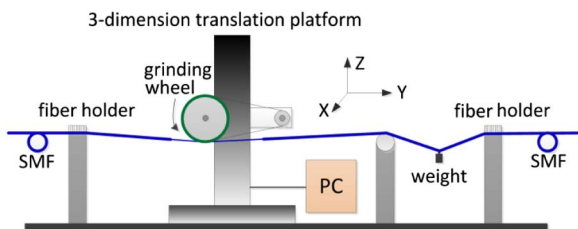


**Fig. 4.** Schematic diagram of the wheel polishing system.

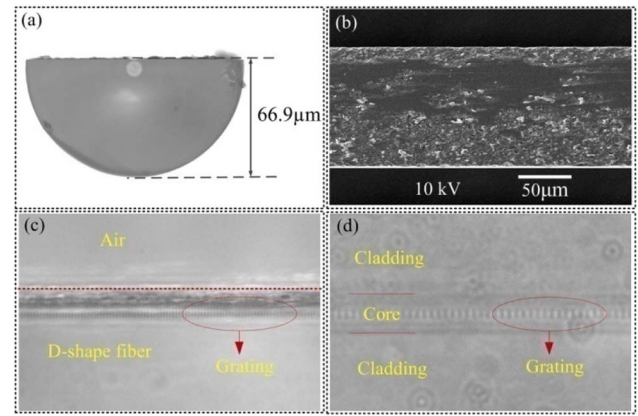


**Fig. 5.** (a) Cross section of the D-shaped fiber; (b) SEM image of the polished fiber surface; (c) side view of the fiber grating structure inscribed in D-shaped fiber; (d) front view of the fiber grating structure in D-shaped fiber.

1567.2 nm, the strength of Bragg resonance is  $\sim 4.6$  dB, and the total insertion loss is  $\sim 24.3$  dB. The significant insertion loss primarily comes from the removal of part of the fiber cladding rather than FBG inscription. As shown in Fig. 6, there are two sets of cladding mode resonances (1st and 2nd order cladding modes) on both sides of the core mode, and the 2nd order cladding mode is more pronounced, and this spectral property is similar with that in Fig. 3. The flatness of the polished surface is not very good, as shown in Fig. 5(b). The poor surface may break the uniformity of each grating segment during laser inscription, leading to spectrum widening and low reflectivity. Moreover, the interference noise caused by FBG inscription becomes notable against the background of large insertion loss.

The RI response of the fabricated D-shaped FBG was investigated at room temperature ( $22^\circ\text{C}$ ). The D-shaped FBG was sequentially immersed into a series of RI oil (Cargille Lab) ranging in RI from 1.360 to 1.450 with an interval of 0.010. Each time the sample was taken out from the tested oil, it should be carefully cleaned with alcohol to completely remove any residual oil. Only if the spectrum returns to the initial state in air, should a new round of testing be performed. Figure 7(a) shows the transmission spectra of the D-shaped FBG immersed

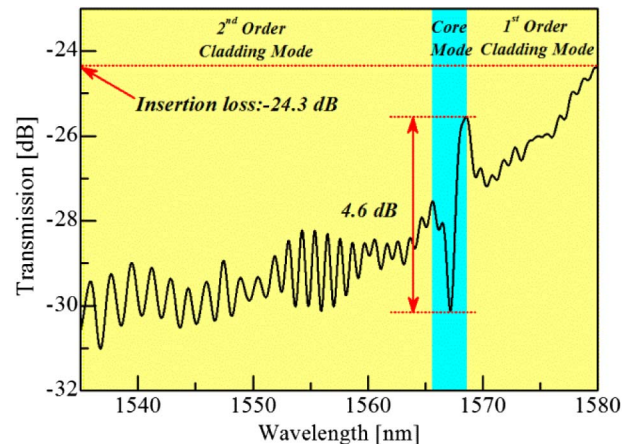


**Fig. 6.** Transmission spectrum of a PBP FBG inscribed in the D-shaped fiber.

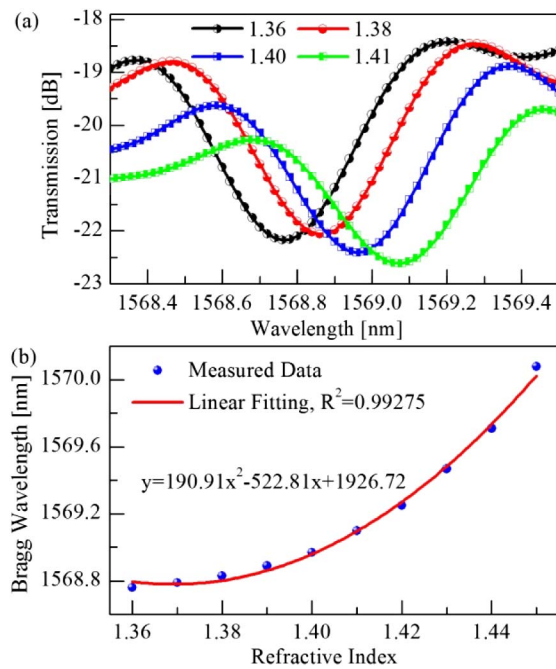


**Fig. 7.** (a) Transmission spectrum evolution of the D-shaped FBG subject to different RI oils; (b) polynomial fitting relationship between Bragg wavelength and the oil RI value.

in oils with RI 1.360, 1.380, 1.400, and 1.410. As shown in this figure, the Bragg wavelength exhibits a significant red shift, and the resonance strength is attenuated with the increase of oil RI. Figure 7(b) shows a polynomial fitting relationship between the Bragg wavelength and the oil RI, where the RI

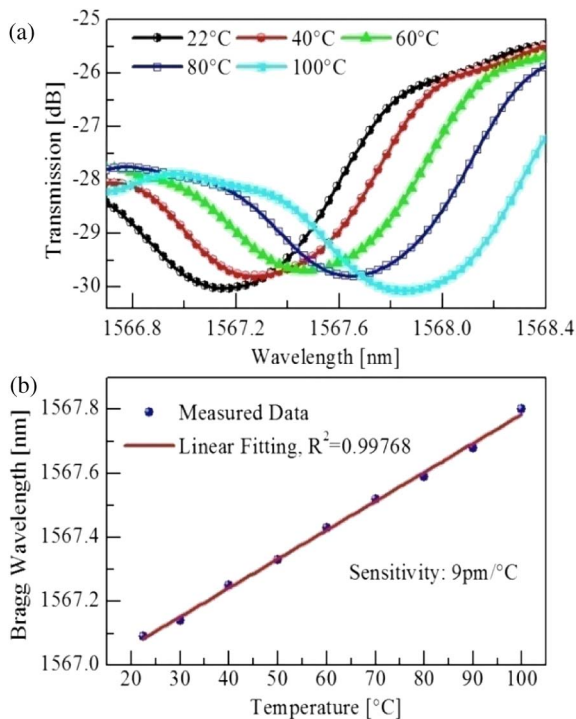


**Fig. 8.** (a) Transmission spectrum evolution of the D-shaped FBG subject to different surrounding temperature; (b) linear fitting relationship between Bragg wavelength and temperature.

sensitivity ( $S$ ) of  $\sim 30$  nm/RIU has been achieved at 1.45. The RI sensitivity of D-shaped FBG reaches an intermediate level of microfiber-based FBGs, i.e., exposed-core-microstructured FBG of 1 nm/RIU [23], suspended-core FBG of 167 nm/RIU [24], and  $\mu$ -FBG of 660 nm/RIU [25]. The limit of detection (LOD) is another important parameter to evaluate the performance of a sensor. The linewidth of the Bragg resonance (full width at half-maximum, FWHM) is  $\sim 0.78$  nm, corresponding to a  $Q$  factor of about 2000. Based on the  $Q$  factor and the sensitivity, the LOD can be obtained [26]:

$$\text{LOD} = \Delta n_{\min} = \frac{\lambda}{QS} = 0.026. \quad (2)$$

The influence of temperature on the D-shaped FBG has also been investigated by placing it in an electric oven and gradually increasing the temperature from 22°C to 100°C. Transmission spectra of the D-shaped FBG at 22°C, 40°C, 60°C, 80°C, and 100°C are shown in Fig. 8(a), where a red shift of Bragg wavelength becomes visible as temperature increases. A linear fitting to the measured data gives a temperature sensitivity of 9 pm/°C, which is similar to those of conventional FBGs. Another important property of ultrashort-laser-induced fiber gratings is the excellent thermal stability. Usually, this type of FBGs is able to withstand temperatures up to 1000°C. Thermal stability of the FBGs is not the research content of this work, and it will be systematically studied later.

#### 4. CONCLUSIONS

This paper demonstrated the fabrication of FBGs using ultrashort pulse laser point-by-point inscription. The laser energy was optimized in SMFs to prevent the self-focusing effect and achieve sufficient reflectivity. Then, FBGs were successfully formed into D-shaped fibers for use as a liquid RI sensor. A nonlinear relationship was observed between the Bragg wavelength and surrounding RI, where the RI sensitivity of  $\sim 30$  nm/RIU was reached at 1.450. The temperature sensitivity of the D-shaped FBGs was found to be 9 pm/°C. Overall, the RI response showed little cross-sensitivity with the temperature of the D-shaped FBG. This offers a considerable advantage over conventional configurations. The device may find new applications in biochemical sensing.

†These authors contributed equally to this work.

**Funding.** National Natural Science Foundation of China (NSFC) (61425007, 61575128, 61308027, 61377090); Guangdong Provincial Science and Technology Department (2014A030308007, 2014B050504010, 2015B010105007, 2015A030313541, 2014A030312008); Science and Technology Innovation Commission of Shenzhen (ZDSYS20140430164957664, KQCX20140512172532195, GJHZ20150313093755757); Pearl River Scholar Fellowships.

#### REFERENCES

1. G. Meltz, W. W. Morey, and W. H. Glenn, "Formation of Bragg gratings in optical fibers by a transverse holographic method," *Opt. Lett.* **14**, 823–825 (1989).
2. B. Malo, K. O. Hill, F. Bilodeau, D. C. Johnson, and J. Albert, "Point-by-point fabrication of micro-Bragg gratings in photosensitive fiber

- using single excimer pulse refractive-index modification techniques," *Electron. Lett* **29**, 1668–1669 (1993).
3. K. O. Hill, B. Malo, F. Bilodeau, D. C. Johnson, and J. Albert, "Bragg gratings fabricated in monomode photosensitive optical fiber by UV exposure through a phase mask," *Appl. Phys. Lett* **62**, 1035–1037 (1993).
  4. A. Martinez, I. Y. Khrushchev, and I. Bennion, "Direct inscription of Bragg gratings in coated fibers by an infrared femtosecond laser," *Opt. Lett* **31**, 1603–1605 (2006).
  5. G. D. Marshall, R. J. Williams, N. Jovanovic, M. J. Steel, and M. J. Withford, "point-by-point written fiber-Bragg gratings and their application in complex grating designs," *Opt. Express* **18**, 19844–19859 (2010).
  6. Y. Lai, K. Zhou, K. Sugden, and I. Bennion, "Point-by-point inscription of first-order fiber Bragg grating for c-band applications," *Opt. Express* **15**, 18318–18325 (2007).
  7. N. Jovanovic, J. Thomas, R. J. Williams, M. J. Steel, G. D. Marshall, A. Fuebach, S. Nolte, A. Tuennermann, and M. J. Withford, "Polarization-dependent effects in point-by-point fiber Bragg gratings enable simple, linearly polarized fiber lasers," *Opt. Express* **17**, 6082–6095 (2009).
  8. J. Burgmeier, C. Waltermann, G. Flachenecker, and W. Schade, "Point-by-point inscription of phase-shifted fiber Bragg gratings with electro-optic amplitude modulated femtosecond laser pulses," *Opt. Lett* **39**, 540–543 (2014).
  9. Y. Lai, A. Martinez, I. Khrushchev, and I. Bennion, "Distributed Bragg reflector fiber laser fabricated by femtosecond laser inscription," *Opt. Lett* **31**, 1672–1674 (2006).
  10. T. Geernaert, K. Kalli, C. Koutsides, M. Komodromos, T. Nasilowski, W. Urbanczyk, J. Wojcik, F. Berghmans, and H. Thienpont, "Point-by-point fiber Bragg grating inscription in free-standing step-index and photonic crystal fibers using near-IR femtosecond laser," *Opt. Lett* **35**, 1647–1649 (2010).
  11. T. L. Lowder, K. H. Smith, B. L. Ipson, A. R. Hawkins, R. H. Selfridge, and S. M. Schultz, "High-temperature sensing using surface relief fiber Bragg gratings," *IEEE Photon. Technol. Lett* **17**, 1926–1928 (2005).
  12. T. L. Lowder, J. D. Gordon, S. M. Schultz, and R. H. Selfridge, "Volatile organic compound sensing using a surface-relief D-shaped fiber Bragg grating and a polydimethylsiloxane layer," *Opt. Lett* **32**, 2523–2525 (2007).
  13. B. C. Yao, Y. Wu, D. J. Webb, J. H. Zhou, Y. J. Rao, A. Pospori, C. B. Yu, Y. Gong, Y. F. Chen, and Z. G. Wang, "Graphene-based D-shaped polymer FBG for highly sensitive erythrocyte detection," *IEEE Photon. Technol. Lett* **27**, 2399–2402 (2015).
  14. Y. Wang, D. N. Wang, M. W. Yang, and C. R. Liao, "Asymmetric microhole-structured long-period fiber gratings," *Sens. Actuators B* **160**, 822–825 (2011).
  15. A. K. Sharma, R. Jha, and B. D. Gupta, "Fiber-optic sensors based on surface plasmon resonance: a comprehensive review," *IEEE Sens. J* **7**, 1118–1129 (2007).
  16. C. R. Liao, T. Y. Hu, and D. N. Wang, "Optical fiber Fabry-Perot interferometer cavity fabricated by femtosecond laser micromachining and fusion splicing for refractive index sensing," *Opt. Express* **20**, 22813–22818 (2012).
  17. Y. Lai, K. Zhou, L. Zhang, and I. Bennion, "Microchannels in conventional single-mode fibers," *Opt. Lett* **31**, 2559–2561 (2006).
  18. R. J. Williams, N. Jovanovic, G. D. Marshall, G. N. Smith, M. J. Steel, and M. J. Withford, "Optimizing the net reflectivity of point-by-point fiber Bragg gratings: the role of scattering loss," *Opt. Express* **20**, 13451–13456 (2012).
  19. A. Couairon and A. Mysyrowicz, "Femtosecond filamentation in transparent media," *Phys. Rep.* **441**, 47–189 (2007).
  20. R. J. Williams, R. G. Kraemer, S. Nolte, M. J. Withford, and M. J. Steel, "Detuning in apodized point-by-point fiber Bragg gratings: insights into the grating morphology," *Opt. Express* **21**, 26854–26867 (2013).
  21. J. Thomas, N. Jovanovic, R. G. Becker, G. D. Marshall, M. J. Withford, A. Tuennermann, S. Nolte, and M. J. Steel, "Cladding mode coupling in highly localized fiber Bragg gratings: modal properties and transmission spectra," *Opt. Express* **19**, 325–341 (2011).
  22. J. Zhao, G. Yin, C. Liao, S. Liu, J. He, B. Sun, G. Wang, X. Xu, and Y. Wang, "Rough side-polished fiber with surface scratches for sensing applications," *IEEE Photon. J.* **7**, 1–7 (2015).
  23. C. Stephen, S. Warren, and M. Tanya, "Exposed core microstructured optical fiber Bragg gratings: refractive index sensing," *Opt. Express* **22**, 1480–1489 (2014).
  24. M. C. Phan, G. Laffont, V. Dewynter, P. Ferdinand, P. Roy, J. L. Auguste, D. Pagnoux, W. Blanc, and B. Dussardier, "Three-hole microstructured optical fiber for efficient fiber Bragg grating refractometer," *Opt. Lett* **32**, 2390–2392 (2007).
  25. Y. Liu, C. Meng, A. P. Zhang, Y. Xiao, H. Yu, and L. Tong, "Compact microfiber Bragg gratings with high-index contrast," *Opt. Lett* **36**, 3115–3117 (2011).
  26. W. Xu, J. Flueckiger, S. Schmidt, S. Grist, S. T. Fard, J. Kirk, M. Doerfler, K. C. Cheung, D. M. Ratner, and L. Chrostowski, "A silicon photonic biosensor using phase-shifted Bragg gratings in slot waveguide," *J. Biophotonics* **6**, 821–828 (2013).